Hindawi
Advances in Materials Science and Engineering
Volume 2022, Article ID 7905927, 19 pages
https://doi.org/10.1155/2022/7905927

Research Article

Study on the Modeling Method and Influencing Parameters of Sandblasting Process for Blade Grinding

Xiangyong Yu, Xiuting Wei, Xuemei Huang, and Leian Zhang

School of Mechanical Engineering, Shandong University of Technology, Zibo 255049, China

Correspondence should be addressed to Xiuting Wei; xiutingwei12315@163.com

Received 1 December 2021; Revised 27 January 2022; Accepted 28 January 2022; Published 9 March 2022

Academic Editor: Fuat Kara

Grinding the surface of wind turbine blades is one of the key production processes before its service. In order to solve the problem of high labor cost and low precision in manual grinding wheel grinding of wind turbine blades, the sandblasting process for blade grinding is proposed. The best parameters of sandblasting process applied to wind turbine blades are investigated by simulation. In this study, the simulation model of sandblasting process is established, and the fluid analysis of blades' grinding using sandblasting process is carried out with the variables of blasting pressure, abrasive diameter, and blast distance. Simulation results show that the best parameters are 0.7 MPa for blasting pressure, 500 mm for spraying distance, and 0.4 mm for abrasive diameter. Finally, the tensile test is carried out on the samples' grind by the traditional grinding process and sandblasting process. The results show that the paint surface grind by sandblasting process can bear a higher load. This study proves the feasibility of the sandblasting process in the composite materials' grinding of wind turbine blades.

1. Introduction

The wind turbine blade, as one of the key components of wind turbines, plays an important role in the stability and efficiency of wind turbines. A series of production processes of the wind turbine blade includes laying glass fiber fabric in the mold, resin dosing, blade demoulding, surface grinding, and painting [1–4]. Good blade paint quality plays a good protective role for the blade against the erosion of a bad working condition [5–7]. Moreover, the blade grinding process determines the paint adhesion. At present, the bulk of the blade manufacturers has adopted the traditional manual grinding method using wheel grinding [8–13]. The manual grinding process not only consumes labor cost due to a bigger and bigger size of the wind turbine blade but also causes paint to drop due to an uneven grinding of the blade surface [14, 15].

However, the sandblasting process can solve this problem. In 1870, Tilghman manufactured a high-pressure jet device. At this time, sandblasting was mostly used for cleaning building surfaces and rusted metal surfaces. In the 20th century, Kirk and Abyaneh [16] studied the influence of coverage on the material surface after sandblasting. Suyitno Arifvianto et al. [17], through microhardness distribution and tensile test results, considered that sandblasting can improve the surface roughness of metal materials and composites. In recent years, in order to study the effect of sandblasting process on material surface roughness, Singh et al. [18] provide a basis for the optimal selection and pressure control of sandblasting technology through test and X-ray methods. Draganovská et al. [19], based on the analysis results, proposed a roughness parameter set that can be used for sandblasting surface evaluation. The above studies are all toward metal material, which proves that sandblasting process can be used for composite materials. The majority evaluation rule of the grinding process is erosion rate and average roughness [20–23].

The sandblasting effect of wind turbine blades is affected by many factors, including abrasive characteristics, sandblasting distance, temperature and humidity of the work condition, blade shape, nozzle length, and airflow pressure. Considering all factors, the research will become complex and difficult. It is not conducive to studying the sandblasting mechanism for the main factors and causes the research to

deviate from the main direction. In the actual sandblasting process, variables with the highest impact are blasting pressure, sandblasting distance, and abrasive diameter [24, 25]. Therefore, this paper mainly studies the influencing parameters and mechanism of these variables on sandblasting process for wind turbine blades.

In this study, the sandblasting process is proposed to replace the traditional manual grinding wheel for blade grinding. The impact of particles on the blade surface makes the blade surface obtain a certain roughness and improves the painting durability of the blade surface. This paper intends to find the best work parameter of the blasting process using simulation, including blasting pressure, sandblasting distance, and abrasive diameter. The hydrodynamic model of blade surface grinding is established, and the influence of different parameters on the grinding process is investigated. Blades' grinding test was established, and the tensile test was carried out with the adhesion of paint on the blade surface after sandblasting as the evaluation standard. Finally, the micromorphology of the blade after grinding was obtained by the scanning electron microscope (SEM) to select the work parameters and study the erosion principle.

2. Test Setup

2.1. Simulation Parameter Setting. Sandblasting belongs to a supersonic jet. According to its working characteristics, it belongs to the category of outflow. Therefore, the boundary of the computational domain needs to be determined artificially. The flow field of sandblasting process is shown in Figure 1. In Figure 1, the nozzle length is 100 mm, the diameter of the nozzle is 6 mm, and the boundary is set as a cylindrical area with a diameter of 800 mm. The nozzle is connected to the compressed air source. The pressure at the nozzle is set as the variable, and the boundary of the computational domain is connected with the atmosphere, and the atmospheric pressure is set as 1.01×10^5 Pa.

According to the classic manual sandblasting process and the working parameters of the actual sandblasting equipment, the pressure (0.5/0.6/0.7/0.8 MPa), abrasive diameter (0.2 mm, 0.3 mm, 0.4 mm, and 0.5 mm), and spraying distance (300 mm, 400 mm, 500 mm, and 600 mm) are selected as variables. Classical values are selected for other parameters in the test, see Table 1 Set the erosion rate and average roughness as the majority evaluation rule. Then, the optimal parameters of sandblasting process are selected by analyzing the erosion of blade surface with different working parameters.

2.2. Test Setup in the Laboratory. Emery is used as sandblasting process medium. The sandblasting equipment is the STR/P-S201408 mobile sandblasting machine produced by Zhangjiagang steer painting equipment Co., Ltd. The test object is the LZ56.8–2.0 blade produced by Lianyungang ZhongfuLianzhong Composite Material Group Co., Ltd. The test area is located 3–5 m from the suction surface of the blade. Within this range, the blade shape is a standard ring shape with a diameter of 2900 mm, which is conducive to the parameter control of the sandblasting test process. The LZ56.8–2.0 blade is the mainstream wind turbine blade in recent years, and it adopts the standard wind turbine blade preparation process in production. The size of a single test area is 600 mm long × 100 mm width × 120 mm spacing.

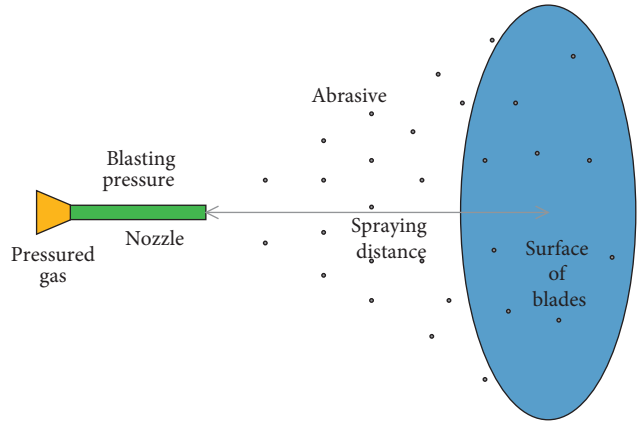

Figure 1: Test setup of sandblasting process.

Table 1: Other working parameters of sandblasting process in simulation.

Parameter	Value
Temperature of compressed air	300 K
Temperature of working environment	300 K
Density of compressed air	7.058 kg/m^3
Atmospheric pressure	1.01×10^5 Pa
Air density	1.225 kg/m^3
Particle density	2600 kg/m^3

3. The Simulation Model of Blade Sandblasting Process

In the model of sandblasting process, the gas is set as the ideal gas, and the sandblasting abrasive is set as spherical solids. The essence of sandblasting is a viscous flow station. The wall of the nozzle adopts the nonslip boundary condition. So, there is no friction and dynamic attenuation between the abrasive and the nozzle wall:

$$\begin{aligned} P \cdot c &= R_i \cdot T, \\ P &= P_0 + P_G, \\ T &= t + 273.2, \end{aligned} \tag{1}$$

where P represents the absolute pressure, and its value is the sum of the external ambient air pressure P_0 during sand blasting and the apparent pressure P_G of the sand blasting equipment. c represents the specific volume of the current gas, and its value is related to the gas density ρ_A is reciprocal to each other. T represents the absolute temperature and t represents the Celsius temperature.

The abrasive of sandblasting is regarded as a single discrete object without volume. According to the different behaviors of abrasive on the wall of the nozzle, their boundary conditions can be divided into reflection

boundary, capture boundary, escape boundary, and wall jet boundary. The reflection boundary assumes that abrasive will reflect the flow field after a collision with the wall. The escape boundary assumes that abrasive will leave the flow field after a collision with the wall. The escape boundary is usually used at the inlet and outlet boundary. According to the working characteristic of the wind turbine blade sandblasting process, the pressure inlet and pressure outlet are set as escape boundaries, and the wall is set as reflection boundary.

Based on the above analysis, the following assumptions are made for the model of wind turbine blades' sandblasting process:

(1) The gas used for sandblasting on the surface of wind turbine blades meets the basic rule of an ideal gas.

(2) The diameter and density distribution of abrasive meets the law of large numbers, and the abrasive is smooth and spherical.

(3) The volume of solid abrasive is negligible compared with that of gas, so the volume of solid abrasive is ignored. At the same time, only the steady-state aerodynamic resistance of continuous relative discrete phase is considered, and the force of discrete relative continuous phase is ignored.

(4) It is assumed that the abrasive is small balls with the same diameter

(5) It is assumed that the abrasive bounce elastically after spraying onto the wall.

(6) Collision between abrasives is not considered.

The model in this study is meshed by Gambit software. The truncation error of the unstructured mesh is larger than that of the structural mesh. Therefore, a structural mesh is used in order to improve the calculation accuracy. For complex geometry, a structural mesh is used near the wall where it has a great impact on the flow, and an unstructured mesh is used in other regions.

The flow described in this study is supersonic flow, and the coupling effect of pressure field and velocity field is strong. Therefore, fluent software is used for simulation. Based on the rule of mass conservation, the mass of the inflow mesh and outflow mesh should be equal to the increment of the fluid mass. Therefore, it can be concluded that the density increment is equal to the integral of the density flux.

The calculation methods of flux include first-order upwind scheme, second-order upwind scheme, and other high-order schemes such as quick scheme. When the first-order upwind scheme is used, the variable value on the boundary is taken as the variable value on the control point of the upstream element. The first-order upwind scheme only retains the first term of the Taylor expansion series. So, it is considered that the value of the boundary point of the local element is equal to the value on the control point of the upstream element, and its scheme accuracy is the first-order accuracy. The second-order upwind scheme retains the first and second terms of the Taylor expansion series. The values on the local boundary points are interpolated by two adjacent element nodes' upstream, which has second-order accuracy. The quick scheme uses the mixed form of weighting and interpolation to give the values on the boundary points. This method is proposed for quadrilateral meshes in two-dimensional and hexahedral meshes in three-dimensional. Although the high-order scheme can bring higher calculation accuracy, it often leads to poor calculation stability and greatly increases the calculation time. Therefore, it is necessary to select the appropriate discrete scheme according to the characteristics of flow. Because the flow described in this study belongs to supersonic flow, the first-order upwind scheme is selected in simulation. The first-order upwind scheme can greatly improve the stability of the calculation with sufficient calculation accuracy.

4. Simulation Results

In order to obtain the optimal working parameters, it is necessary to simulate and calculate three cases: different blasting pressures, different spraying distances, and different abrasive diameters. Then, explore the influence mechanism of these parameters on the erosion rate and average roughness.

4.1. Simulation Results of Case 1: Different Blasting Pressures. Set the blasting pressure as variable; the distance from the nozzle to the blade surface is 500 mm, and the abrasive diameter is 0.2 mm. Figure 2 is the simulation results of gas velocity with the blasting pressure of 0.5 MPa, 0.6 MPa, 0.7 MPa, and 0.8 MPa. Take the result of blasting pressure with 0.5 MPa in Figure 2(a) as an example. It can be seen that the compressed gas continuously accelerates inside the nozzle, and the gas reaches the maximum speed outside the nozzle outlet, about 450 m/s. Then, the gas velocity decreases rapidly. When it reaches 300 mm from the blade surface, the velocity has been reduced to only tens. The gas will continue to accelerate inside the nozzle due to the nozzle effect. When the high-pressure gas is sprayed out of the nozzle, the gas will still accelerate for a distance under the action of expansion. However, at this time, the potential core has been formed, and the compressed gas begins to interact with the ambient gas due to velocity slip. With the mutual coupling between compressed gas and ambient gas, the potential nuclear effect of compressed gas gradually decreases and finally disappears, so the velocity begins to decrease rapidly. The results of the blasting pressure with 0.6 MPa, 0.7 MPa, and 0.8 MPa still show the same trend. However, at the same acceleration distance, it can be found that the velocity of compressed gas increases with the increase of pressure.

Figure 3 shows the results of the average shear stress distribution in blade surface when the blasting pressure is 0.5 MPa, 0.6 MPa, 0.7 MPa, and 0.8 MPa. Take the result of shear stress distribution in blade surface with a blasting pressure of 0.5 MPa in Figure 3(a) as an example. It can be seen from the result that the shear stress distribution in the blade surface is circular. This is because of the potential nucleation, resulting in a relatively high gas velocity in the

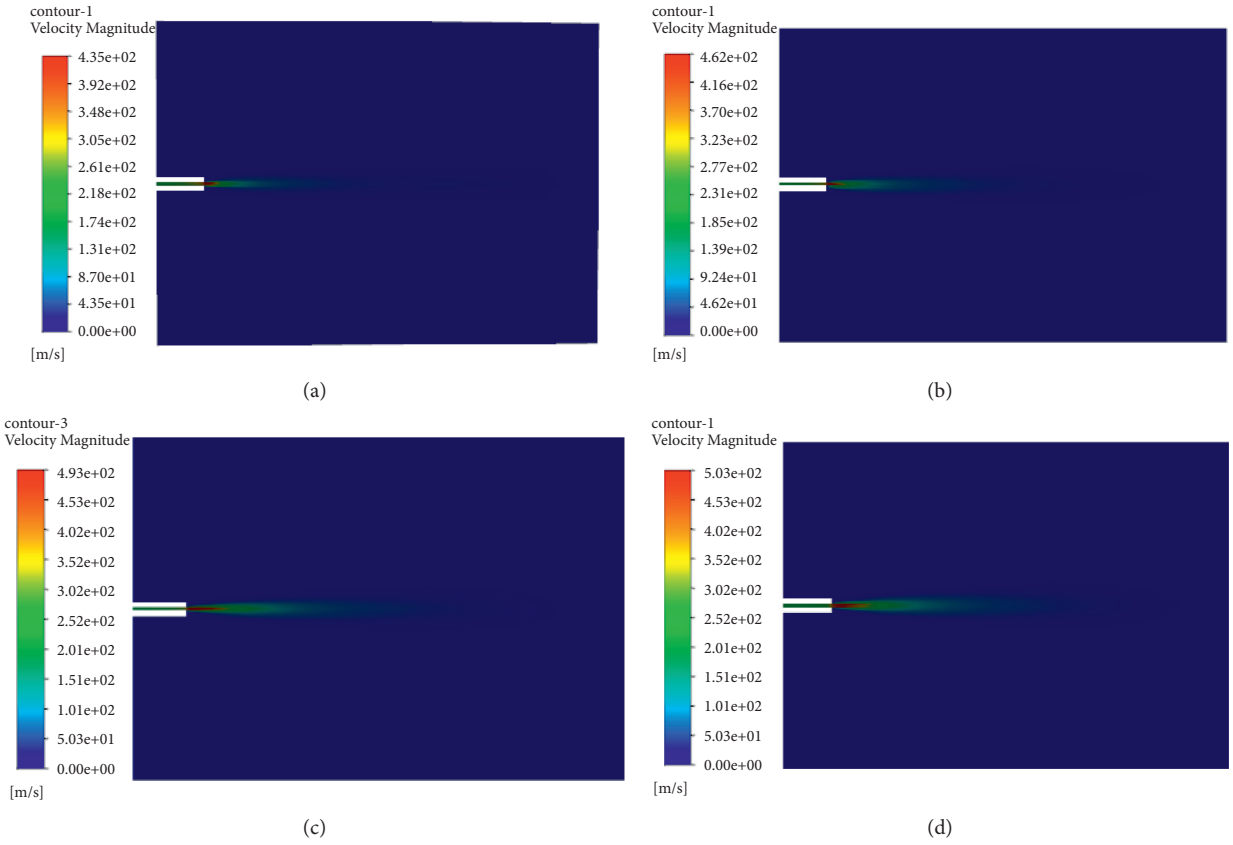

Figure 2: Results of gas velocity with different blasting pressures. (a) Results of gas velocity with the blasting pressure of 0.5 MPa. (b) Results of gas velocity with the blasting pressure of 0.6 MPa. (c) Results of gas velocity with the blasting pressure of 0.7 MPa. (d) Results of gas velocity with the blasting pressure of 0.8 MPa.

center of the nozzle, and abrasives will be blown vertically to the blade surface. Therefore, high forward pressure will be generated in the center of the blade surface, and the tangential force is low. Due to the expansion, the flow outside the central has a certain inclination with the blade surface, and the gas has a certain tangential flow. Therefore, the abrasive will produce a high shear force on the blade surface.

The results of shear stress distribution on the blade surface with the blasting pressure of 0.6 MPa, 0.7 MPa, and 0.8 MPa are similar to the blasting pressure of 0.5 MPa. When the pressure is less than 0.7 MPa, the shear force on the blade surface is also distributed in a ring. However, with the increase of blasting pressure, more high-speed abrasives arrive at the blade surface. As a result, the proportion of the high positive pressure region (dark blue area) and the high tangential force ring (dark red area) in the central area began to increase. When the pressure is higher than 0.7 MPa, the strength of the jet increases, and the convergence of the central gas is stronger, resulting in a lower proportion of the high positive pressure region (dark blue area). With the increase of abrasives velocity, the abrasives' beam is more concentrated. Therefore, the proportion of the high tangential force ring caused by the expansion of external gas is also gradually reduced.

Figure 4 shows the results of the gas pressure distribution along the axis with the blasting pressure of 0.5 MPa, 0.6 MPa, 0.7 MPa, and 0.8 MPa. Take the result of gas pressure distribution along the axis with a blasting pressure of 0.5 MPa as an example. It can be seen from the result that the gas pressure presents a slow decline process at the nozzle outlet. When the high-pressure gas is ejected from the nozzle for a certain distance, the pressure decreases rapidly. This result further explains the development characteristic of the reduction of the pressure potential core when it leaves the nozzle. It can be seen from the trend of the gas pressure distribution along the axis when the blasting pressure is 0.5 MPa, 0.6 MPa, 0.7 MPa, and 0.8 MPa. The higher gas pressure will drive abrasive to produce a higher sandblasting speed and a greater erosion on the blade surface.

Figure 5 shows the results of abrasive velocity distribution along the axis with the blasting pressure of 0.5 MPa, 0.6 MPa, 0.7 MPa, and 0.8 MPa. Take the results of abrasive velocity distribution along the axis with the blasting pressure of 0.5 MPa as an example. It can be seen that the abrasive velocity is continuously increased due to the continuous expansion of compressed gas and then is turned down rapidly after reaching the peak. Although the gas pressure is decreasing, the acceleration of the abrasive is still positive in this process, resulting in an increase in the velocity of the abrasive. When the potential core of compressed gas decreases to a certain extent, the acceleration of the abrasive decreases below zero and the velocity of the abrasive

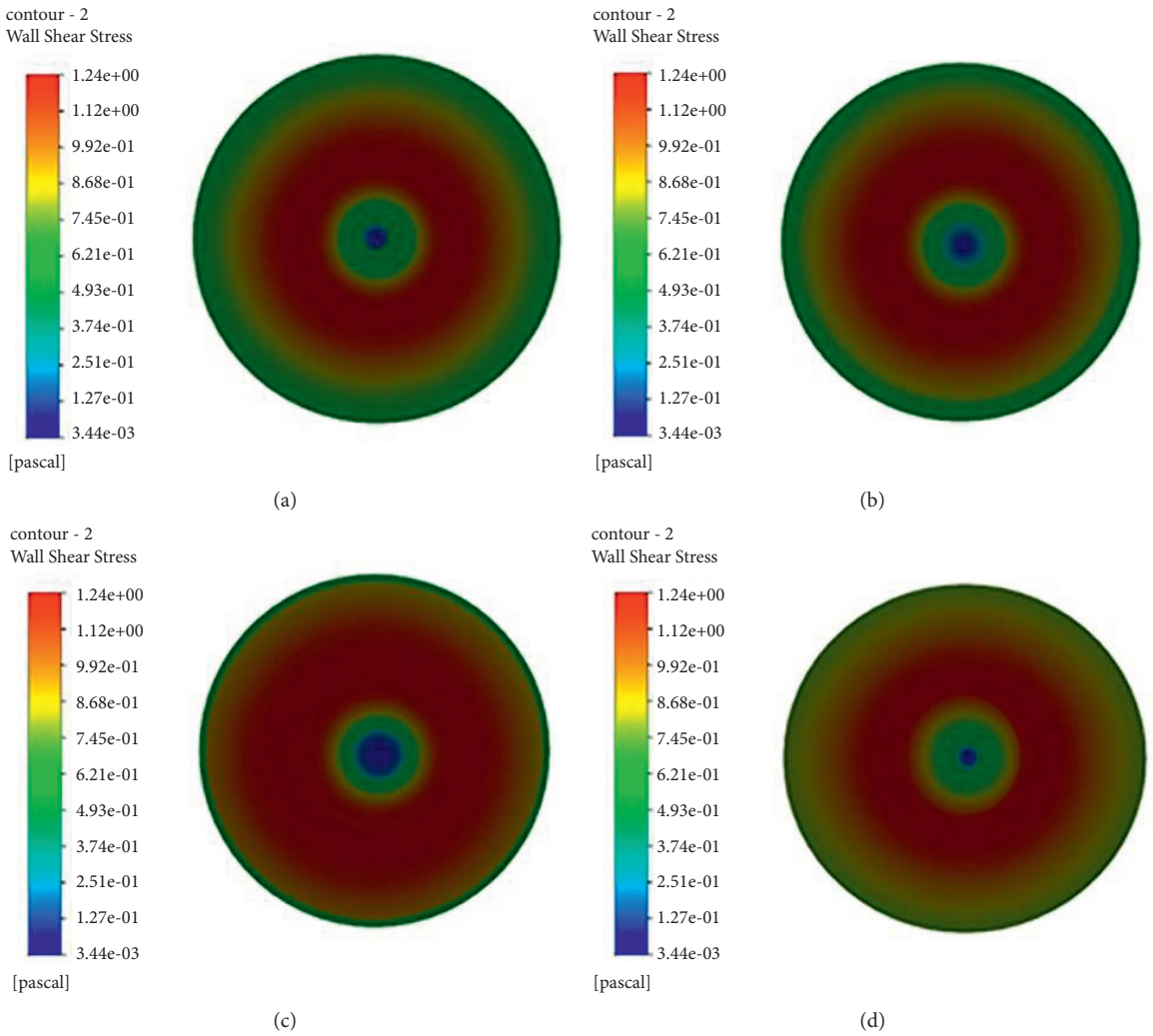

Figure 3: The results of shear stress distribution on the blade surface with different blasting pressures. (a) The shear stress distribution with the blasting pressure of 0.5 MPa. (b) The shear stress distribution with the blasting pressure of 0.6 MPa. (c) The shear stress distribution with the blasting pressure of 0.7 MPa. (d) The shear stress distribution with the blasting pressure of 0.8 MPa.

decreases rapidly. With the continuous reduction of the gas pressure, the differential pressure between the gas pressure and the ambient pressure gradually decreases. Therefore, in the end, the flow rate of the abrasive decreases rapidly. The velocity distribution of abrasive along the axis with the blasting pressure of 0.6 MPa, 0.7 MPa, and 0.8 MPa also has the same trend. The difference is that, with the increase of blasting pressure, the maximum velocity increases, and the velocity when reaching the blade surface also increases. This proves that increasing the blasting pressure is conducive to improving the speed of axial abrasives when they reach the working face. It also increases the kinetic energy of abrasive and improves the erosion of abrasive on the blade surface.

Figure 6 shows the erosion results of the blade surface with the blasting pressure of 0.5 MPa, 0.6 MPa, 0.7 MPa, and 0.8 MPa. Take the erosion results of the blade surface with the blasting pressure of 0.5 MPa as an example. It can be seen that erosion occurs in the central ring of the jet. From the shape of the erosion, it is mainly circular, which is basically consistent with the shear force distribution. At the same time, it can be concluded that erosion is mainly caused by high central forward pressure and high-speed tangential force. Erosion mainly occurs in the middle and is relatively evenly distributed, which is conducive to planning and controlling the sandblasting path.

The distribution of erosion with blasting pressure of 0.6 MPa, 0.7 MPa, and 0.8 MPa is consistent with the results of 0.5 MPa. It can be seen that when the blasting pressure is lower than 0.7 MPa, the erosion rate per unit region increases with the increase of pressure and tends to be uniform. When the blasting pressure is higher than 0.7 MPa, the erosion rate per unit area decreases with the increase of pressure. This phenomenon is consistent with the shear force distribution in the blade surface. When the blasting pressure is lower than 0.7 MPa, the velocity of abrasive increases with the increase of pressure. Then, the kinetic energy of abrasive increases and more abrasives arrive at the surface in unit time. When the blasting pressure is higher than 0.7 MPa, although the flow velocity of abrasive is accelerated and the kinetic energy of abrasive particles is increased, the central

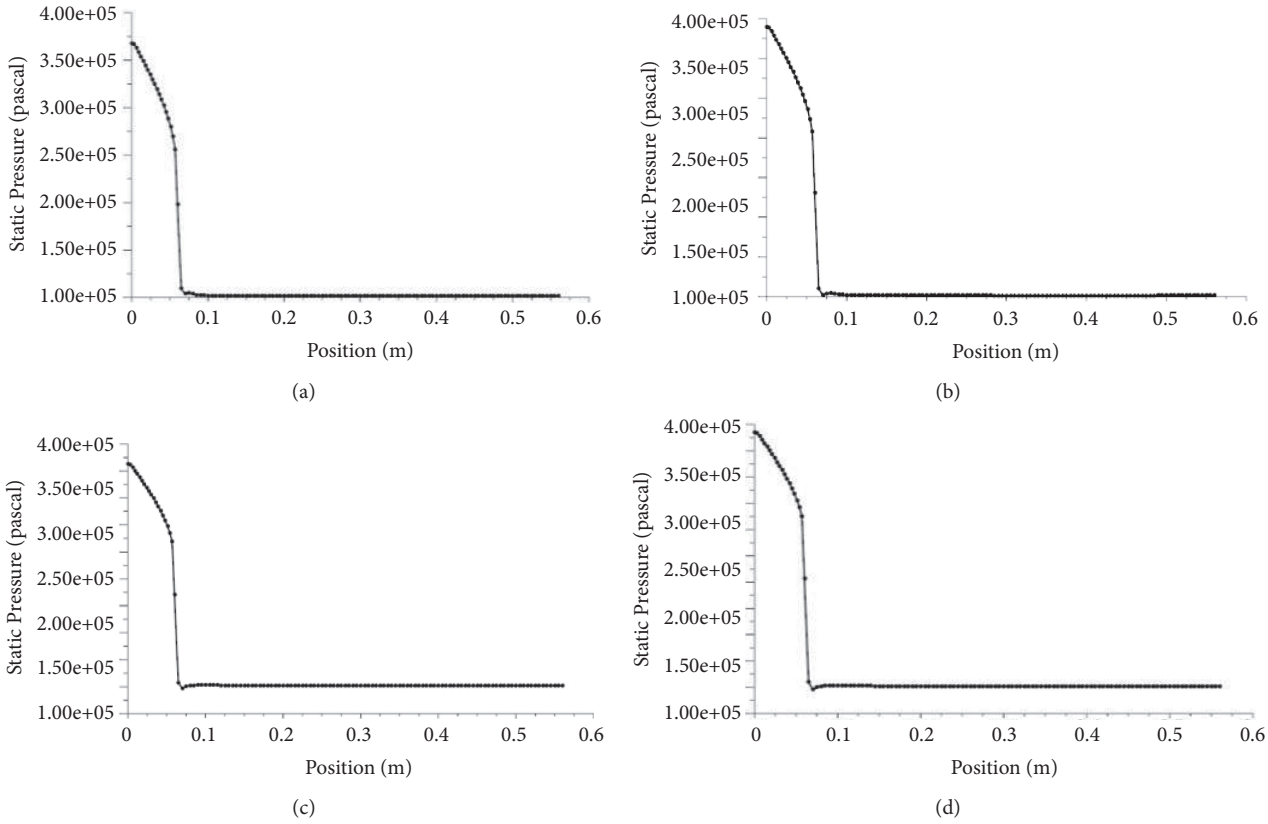

Figure 4: The results of gas pressure distribution along the axis with different blasting pressures. (a) The gas pressure distribution along the axis with the blasting pressure of 0.5 MPa. (b) The gas pressure distribution along the axis with the blasting pressure of 0.6 MPa. (c) The gas pressure distribution along the axis with the blasting pressure of 0.7 MPa. (d) The gas pressure distribution along the axis with the blasting pressure of 0.8 MPa.

particle beam is more concentrated. This results in the shrinkage of the proportion of high erosion regions.

Figure 7 shows the trajectory results of the abrasive with the blasting pressure of 0.5 MPa, 0.6 MPa, 0.7 MPa, and 0.8 MPa. Take the abrasive trajectory with the blasting pressure of 0.5 MPa as an example. It can be seen that the abrasive in the center is perpendicular to the blade surface, and the peripheral abrasive have a certain included angle with the blade surface, which provides an explanation for the generation mechanism of the shear force distribution. When the blasting pressure is below 0.7 MPa, the erosion region caused by high forward pressure and high shear force gradually expands with the increase of pressure, and the central flow beam of abrasive gradually diffuses. When the blasting pressure exceeds 0.7 MPa, the central flow beam converges with the increase of pressure, and the proportion of erosion region caused by high forward pressure and high shear force begins to decrease. The above characters are the same as the generation mechanism of shear stress distribution and erosion results. It can achieve the purpose of mutual evidence. At the same time, according to Figure 7, with the change of blasting pressure, the effective erosion region, average erosion rate, and maximum erosion rate have changed.

Figure 8 shows the erosion curve of the transverse blade surface with the blasting pressure of 0.5 MPa, 0.6 MPa, 0.7 MPa, and 0.8 MPa. It can be seen from the curve that the influence of blasting pressure on the erosion region is limited, but the proportion of the high erosion rate region changes significantly with the change of blasting pressure.

When the blasting pressure is less than 0.7 MPa, both the maximum erosion rate and the average erosion rate are increasing. Moreover, it can be seen from the comparison that, within this range, the number of erosion rate peaks decreases, and the change tends to be gentle. This is because, within a certain blasting pressure, with the increase of blasting pressure, more and more abrasives have been accelerated, and more abrasive have reached the blade surface.

When the blasting pressure is 0.7 MPa, the maximum erosion rate and average erosion rate reach the maximum. At this time, the abrasives are fully accelerated and have higher kinetic energy.

When the blasting pressure is greater than 0.7 MPa, the maximum erosion rate and average erosion rate decline significantly. As shown in the trajectory results of abrasive, the abrasive flow beam converges more with the increase of blasting pressure, so the regions of high forward pressure and high shear force decrease.

In order to compare the erosion of abrasive on the blade surface under different pressures, the average roughness values of the blade surface under eight pressure points are

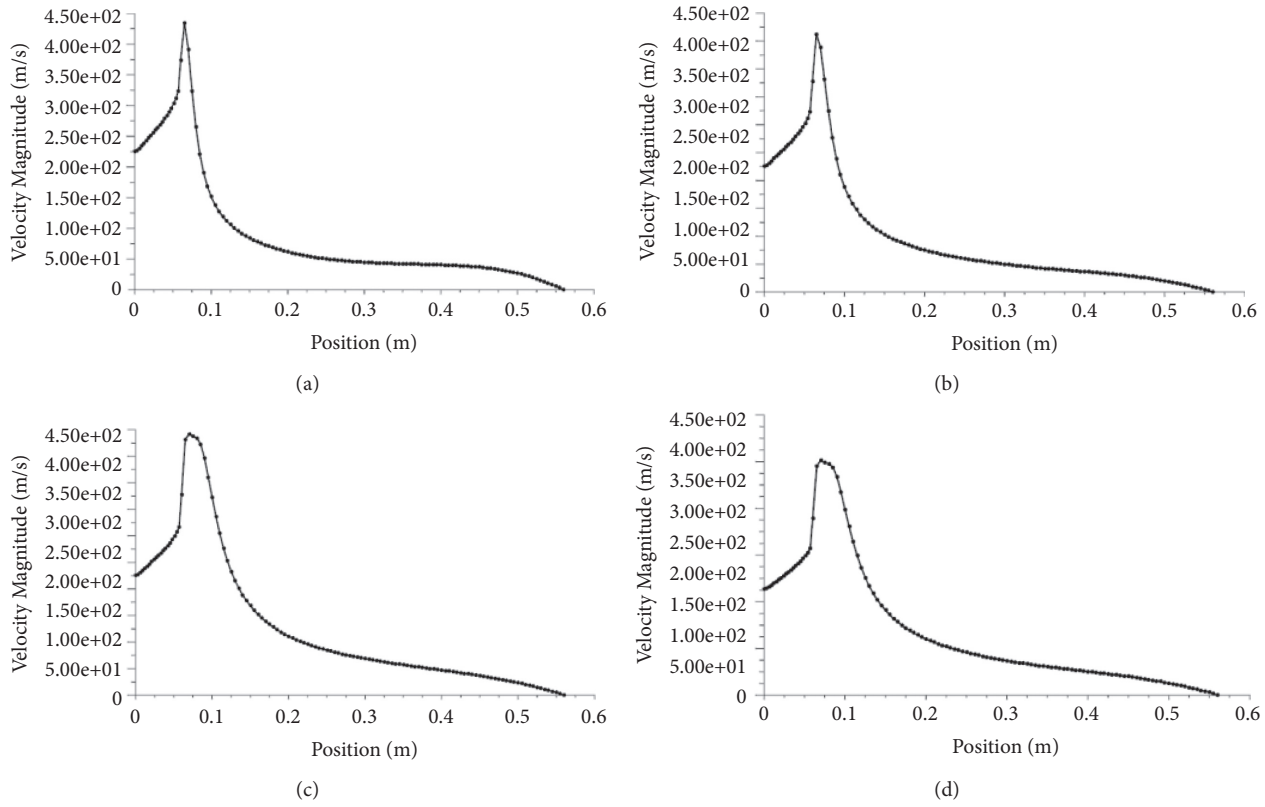

Figure 5: The results of abrasive velocity distribution along the axis with different blasting pressures. (a) The abrasive velocity distribution along the axis with the blasting pressure of 0.5 MPa. (b) The abrasive velocity distribution along the axis with the blasting pressure of 0.6 MPa. (c) The abrasive velocity distribution along the axis with the blasting pressure of 0.7 MPa. (d) The abrasive velocity distribution along the axis with the blasting pressure of 0.8 MPa.

measured and counted in the simulation software, see Figure 9.

It can be seen from Figure 9 that the trend is basically consistent with the macroform analyzed above. When the blasting pressure is below 0.7 MPa, the higher the blasting pressure, the higher the jet intensity. Then, the higher the kinetic energy of abrasive particles when they reach the jet surface, the higher the average roughness value. However, when the blasting pressure is above 0.7 MPa, the larger the blasting pressure is, the smaller the average roughness value is. This is because the higher the blasting pressure, the higher the jet intensity and the more compact the flow beam. A large number of abrasives erode the same region, resulting in excessive sandblasting time, which is not conducive to the growth of roughness.

4.2. Simulation Results of Different Spraying Distances. When the spraying distance changes and other conditions remain unchanged, the flow field and erosion results with the spraying distance of 300 mm, 400 mm, 500 mm, and 600 mm are analyzed, respectively. In the simulation, the blasting pressure is 0.7 MPa and the abrasive diameter is 0.2 mm.

Figure 10 shows the average shear stress distribution of the blade surface with the spraying distance of 300 mm, 400 mm, 500 mm, and 600 mm. Take the shear force distribution result with a spraying distance of 300 mm as an example. It can be seen that the shear force distribution is circular. This is due to the existence of a potential core, resulting in relatively high gas velocity in the center of the nozzle. High gas velocity will blow the abrasive vertically to the blade surface, resulting in large positive pressure on the abrasive in the center of the blade surface. However, the tangential force (shear force) is low. Similarly, due to the expansion of the flow outside the central airflow, the gas produces a certain tangential slip, resulting in a certain inclination of the outer abrasive acting on the blade surface. Therefore, the blade surface will suffer a high shear force, but low forward pressure.

For the shear force distribution at the blade surface with spraying distances of 400 mm, 500 mm, and 600 mm, the shear force on the blade surface is also distributed in a ring. However, in the range of 300–500 mm, due to the increase of spraying distance, the gas can fully expand and accelerate, and more high-speed abrasive particles reach the blade surface. At the same time, with the increase of distance, the total erosion area increases because the jet is horn-shaped. The above two reasons lead to the expansion of the area proportion of central high forward pressure region and high tangential force region. At 500 mm–600 mm, under the same pressure, the abrasive will be fully accelerated if the spraying

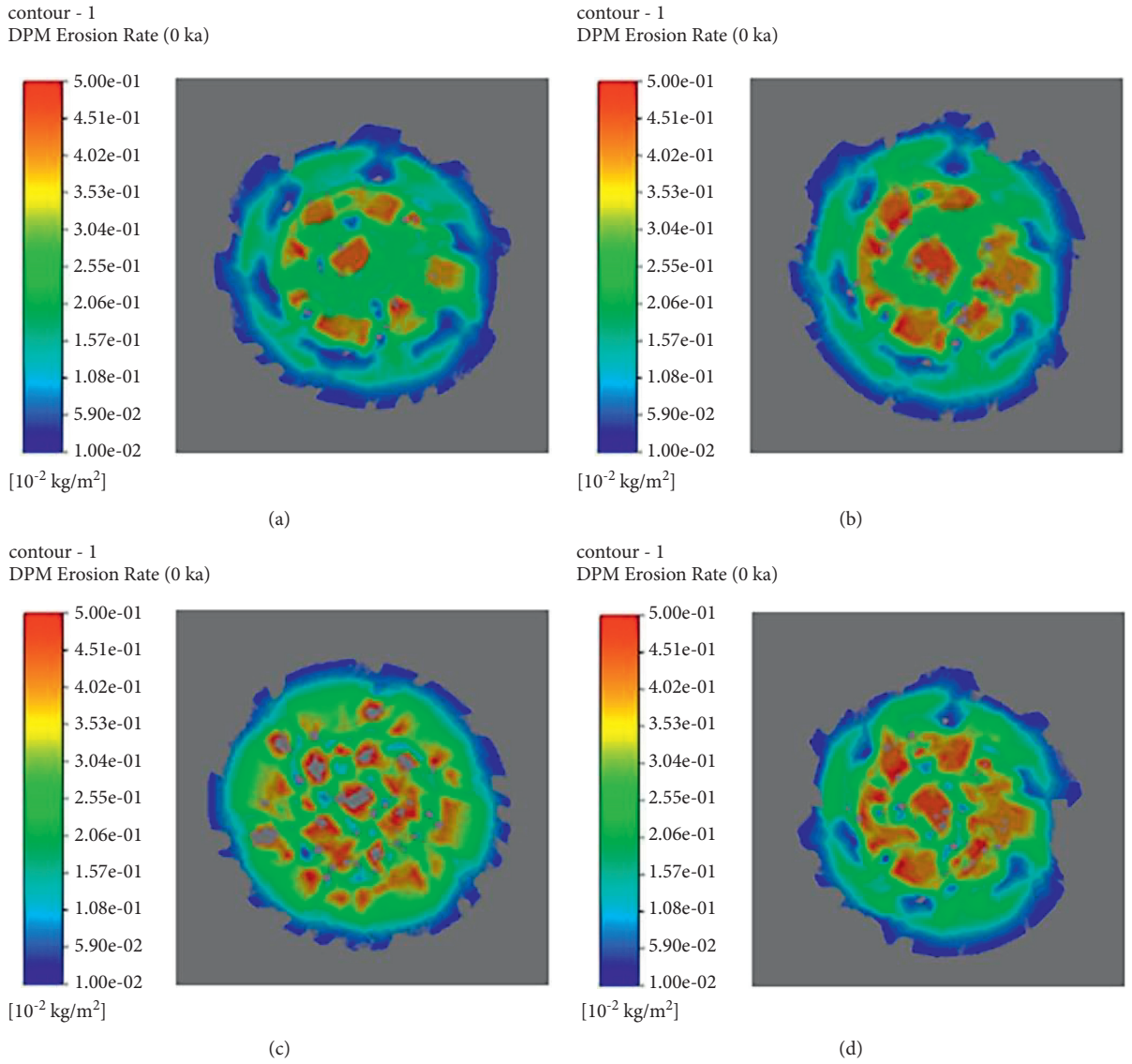

Figure 6: The erosion results of the blade surface with different blasting pressures. (a) The erosion of the blade surface with the blasting pressure of 0.5 MPa. (b) The erosion of the blade surface with the blasting pressure of 0.6 MPa. (c) The erosion of the blade surface with the blasting pressure of 0.7 MPa. (d) The erosion of the blade surface with the blasting pressure of 0.8 MPa.

distance is appropriately lengthened. However, if the blasting distance is too long, the airflow pressure will decrease, and the abrasive will decelerate under the action of external gas. Abrasive deceleration reduces the number of abrasive on the central axis and outer ring reaching the blade surface.

Figure 11 shows the erosion of the blade surface after the same sandblasting time with the spraying distance of 300 mm, 400 mm, 500 mm, and 600 mm. Take the erosion of the blade surface at the jet distance of 300 mm as an example. It can be seen that erosion mainly occurs in the central ring of the jet. From the shape of the erosion results, it is mainly circular, which is basically consistent with the law of shear force distribution at different spraying distances. At the same time, it can be seen that erosion is mainly caused by forwarding pressure and high-speed tangential force. Erosion mainly occurs in the middle and is relatively evenly distributed, which is conducive to realizing the uniform position of sandblasting coverage.

The development law of the erosion results of the blade surface is consistent with the above analysis when the spraying distance is 400 mm, 500 mm, and 600 mm. It can be seen that when the spraying distance is less than 500 mm, the erosion rate per unit area increases with the extension of the distance. However, it is accompanied by an obvious circumferential saw tooth edge with an ultra-low erosion rate. The generation mechanism of ultra-low erosion rate circular saw tooth edge is that the spraying distance is short, and the abrasive in the outer layer cannot fully accelerate and expand. This results in small kinetic energy, so this phenomenon occurs.

When the spraying distance is 500 mm, the erosion rate is the maximum, the abrasive has been fully expanded and

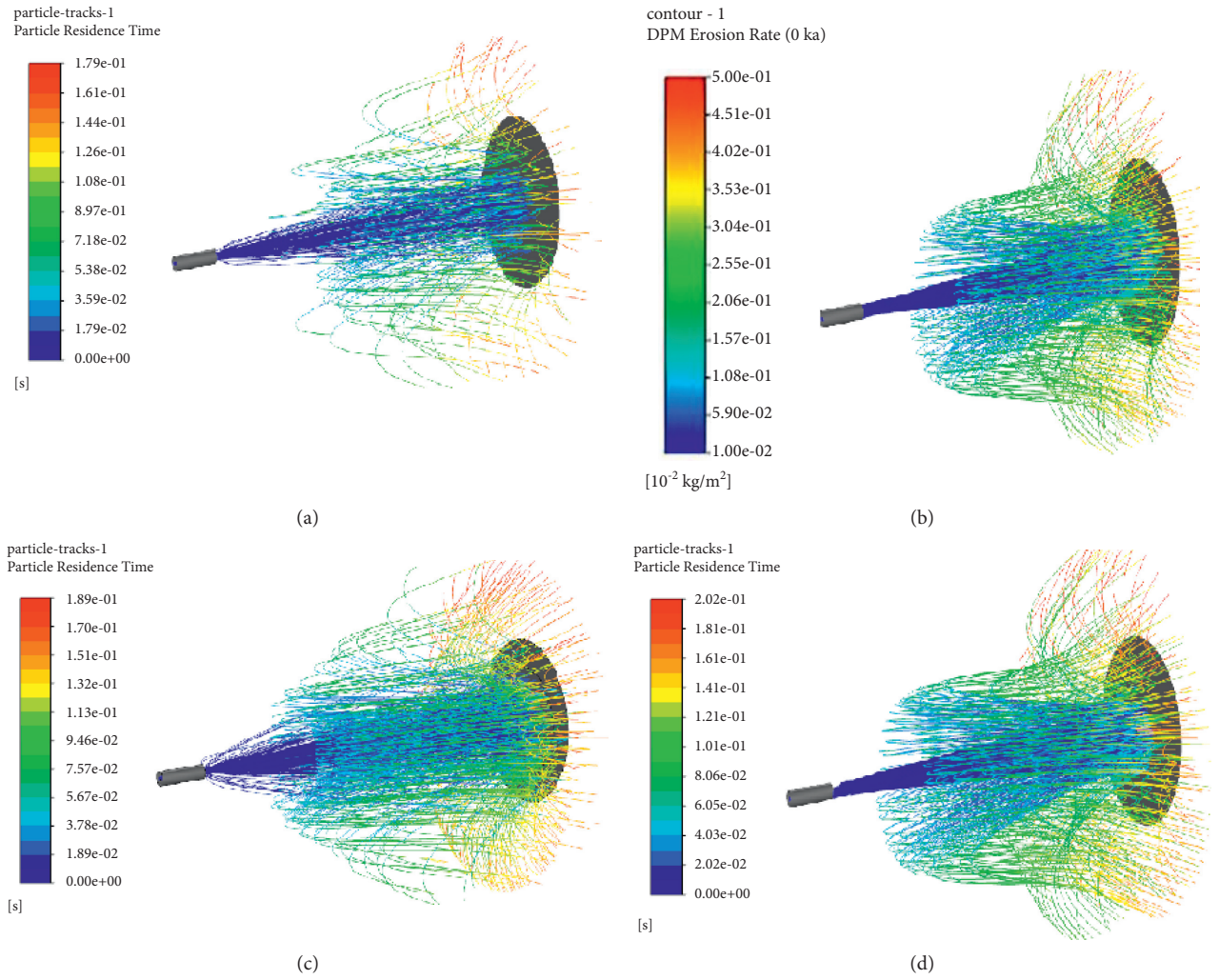

Figure 7: The trajectory results of the abrasive with different blasting pressure. (a) The trajectory of the abrasive with the blasting pressure of 0.5 MPa. (b) The trajectory of the abrasive with the blasting pressure of 0.6 MPa. (c) The trajectory of the abrasive with the blasting pressure of 0.7 MPa. (d) The trajectory of the abrasive with the blasting pressure of 0.8 MPa.

accelerated, and the circumferential saw tooth edge of the ultra-low erosion rate almost disappears.

However, when the sandblasting distance exceeds 500 mm, the erosion rate per unit area decreases with the extension of the distance. This phenomenon is consistent with the shear force distribution in the blade surface. It is, due to the increase of blasting distance, the acceleration of abrasive becomes negative, and the flow velocity of abrasive decreases due to the resistance of external gas. At the same time, the number of abrasives reaching the blade surface is also greatly reduced with the increase of distance, especially the abrasive in contact with the environment in the outer layer. All the particles that can reach the blade surface are low-speed abrasive. Therefore, the outer layer has a circumferential saw tooth edge with an ultra-low erosion rate.

Figure 12 shows the erosion curve of the blade surface with the spraying distance of 300 mm, 400 mm, 500 mm, and 600 mm. It can be seen that both the maximum erosion rate and the average erosion rate are increasing in the range of spraying distance of 300–500 mm. Moreover, it can be seen from the comparison of curves that, within this range, the area of the ultra-low erosion region decreases, and the change tends to be gentle. This is because, within a certain spraying distance, with the increase of spraying distance, more abrasives have been accelerated, and more abrasive have reached the blade surface. When the spraying distance is 500 mm, it reaches the maximum value, and the maximum erosion rate and average erosion rate reach the maximum value. At this time, the abrasive is fully accelerated and has higher kinetic energy. However, the maximum erosion rate and average erosion rate decreased significantly at 500 mm–600 mm. As shown in the shear force distribution and jet distance, with the increase of jet distance, the gas is fully expanded, which leads to the higher kinetic energy of abrasive. However, after the gas reaches the maximum velocity under this pressure, the gas potential core disappears and the velocity will decrease significantly. Finally, the erosion rate of abrasive particles on the working face decreases significantly.

In order to compare the erosion of abrasive on the blade surface more intuitively under different spraying distances,

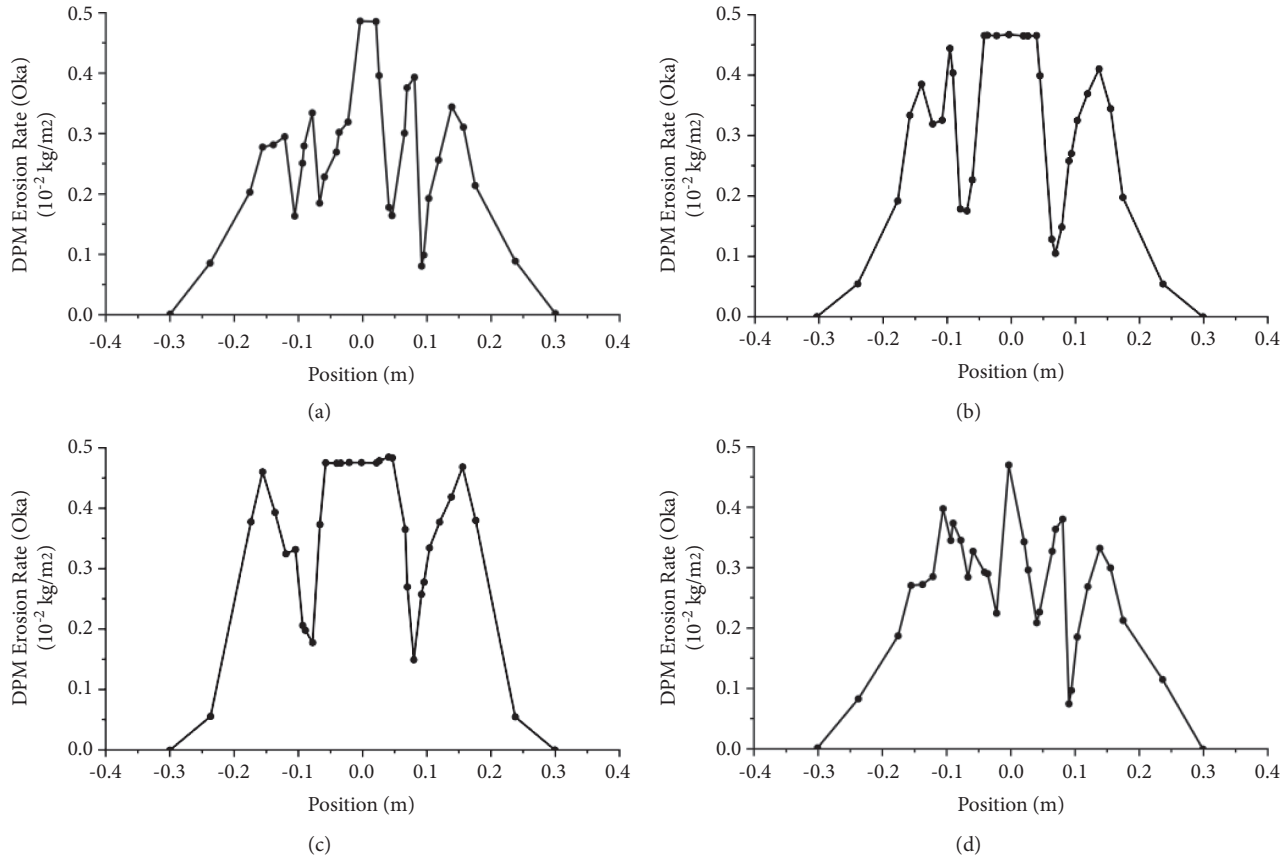

Figure 8: The erosion curve of the transverse blade surface with different blasting pressures. (a) The erosion curve of the transverse blade surface with the blasting pressure of 0.5 MPa. (b) The erosion curve of the transverse blade surface with the blasting pressure of 0.6 MPa. (c) The erosion curve of the transverse blade surface with the blasting pressure of 0.7 MPa. (d) The erosion curve of the transverse blade surface with the blasting pressure of 0.8 MPa.

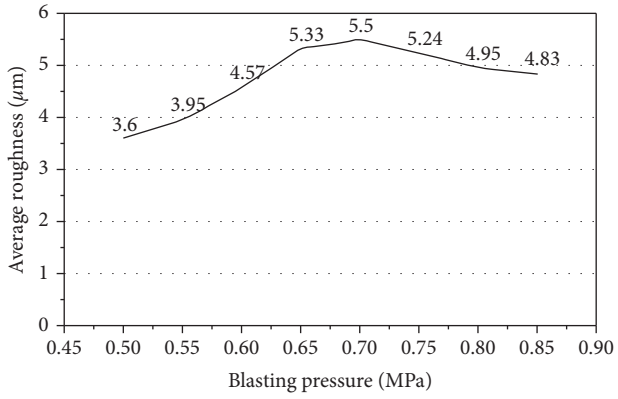

Figure 9: Average roughness curve of the blade surface with different blasting pressures.

the average roughness corresponding to eight injection distances is measured and counted in the simulation software. Finally, the curve is generated, see Figure 13.

When the spraying distance is less than 500 mm, the larger the spraying distance is, the higher the average roughness value is. This is because, with the larger spraying distance, the airflow can fully expand and fully accelerate the abrasive. When the abrasive reaches the jet surface, the greater the kinetic energy they have.

When the spraying distance is more than 500 mm, the larger the spraying distance is, the average roughness value decreases slowly. Although the airflow has fully accelerated the abrasive, in the later stage of the abrasive movement, the pressure of the compressed gas gradually decreases. The

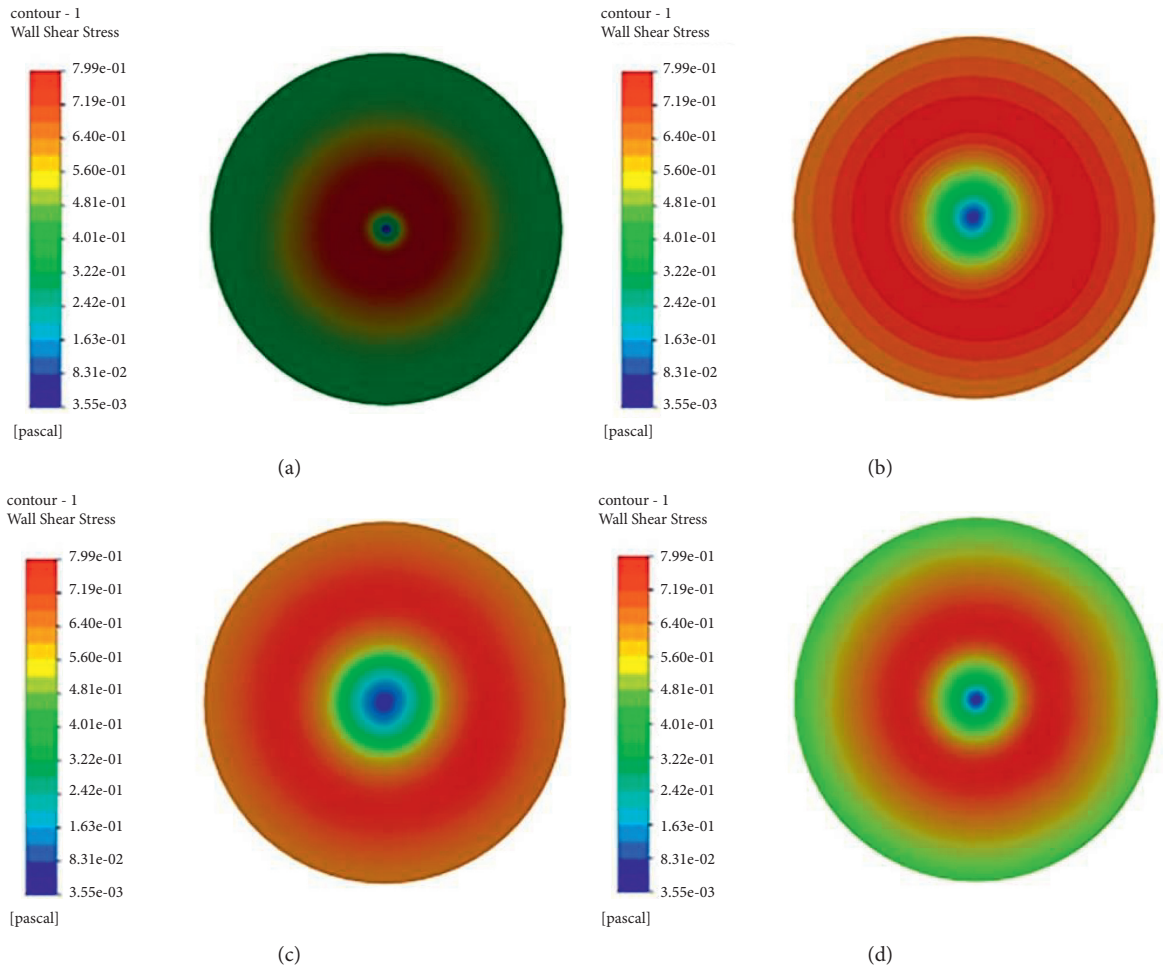

Figure 10: The results of the shear force distribution with different spraying distances. (a) The shear force distribution with spraying distances of 300 mm. (b) The shear force distribution with spraying distances of 400 mm. (c) The shear force distribution with spraying distances of 500 mm. (d) The shear force distribution with spraying distances of 600 mm.

speed of the abrasive decreases rapidly, and the kinetic energy of the abrasive decreases, resulting in the simultaneous reduction of erosion rate and roughness.

4.3. Simulation Results of Different Abrasive Diameters. When the abrasive diameter changes and other conditions remain unchanged, the flow field and erosion results are calculated, respectively, when the abrasive diameter is 0.2 mm, 0.3 mm, 0.4 mm, and 0.5 mm, in which the distance from the nozzle to the blade surface is 500 mm and the blasting pressure is 0.7 MPa.

Figure 14 shows the results of the average shear force distribution of the blade surface when the abrasive diameter is 0.2 mm, 0.3 mm, 0.4 mm, and 0.5 mm. Take the cloud diagram of shear force distribution of the blade surface with an abrasive diameter of 0.2 mm as an example. It can be seen that the shear force distribution is circular. Due to the existence of a potential core, the air velocity in the center of the nozzle is relatively high. The abrasive will be blown vertically to the blade surface, resulting in large positive pressure on the center of the blade surface, and the tangential force (shear force) is very small. Similarly, due to the expansion of the flow outside the central airflow, the gas produces a certain tangential slip, resulting in a certain inclination of the outer abrasive acting on the blade surface. Therefore, a high shear force will be generated on the blade surface, and the forward pressure is low.

Figure 14 shows the results of shear force distribution on the blade surface with the abrasive diameter of 0.3 mm, 0.4 mm, and 0.5 mm; the shear force on the blade surface is also distributed in a ring. In the range of 0.2–0.4 mm, the proportion of positive pressure and high shear force increases in the shear force distribution of the blade surface. Due to the increase of abrasive diameter and the increase of the upwind force region of the unit particle, abrasive will receive a higher driving force, resulting in greater kinetic energy when the unit particle reaches the working face. However, the proportion of positive pressure and high shear force decreases when the abrasive diameter exceeds 0.4 mm. With the increase of abrasive diameter, the airflow force increases. However, the mass of abrasives also increases, and the number of abrasives reaching the working face per unit time decreases, resulting in the reduction of erosion rate.

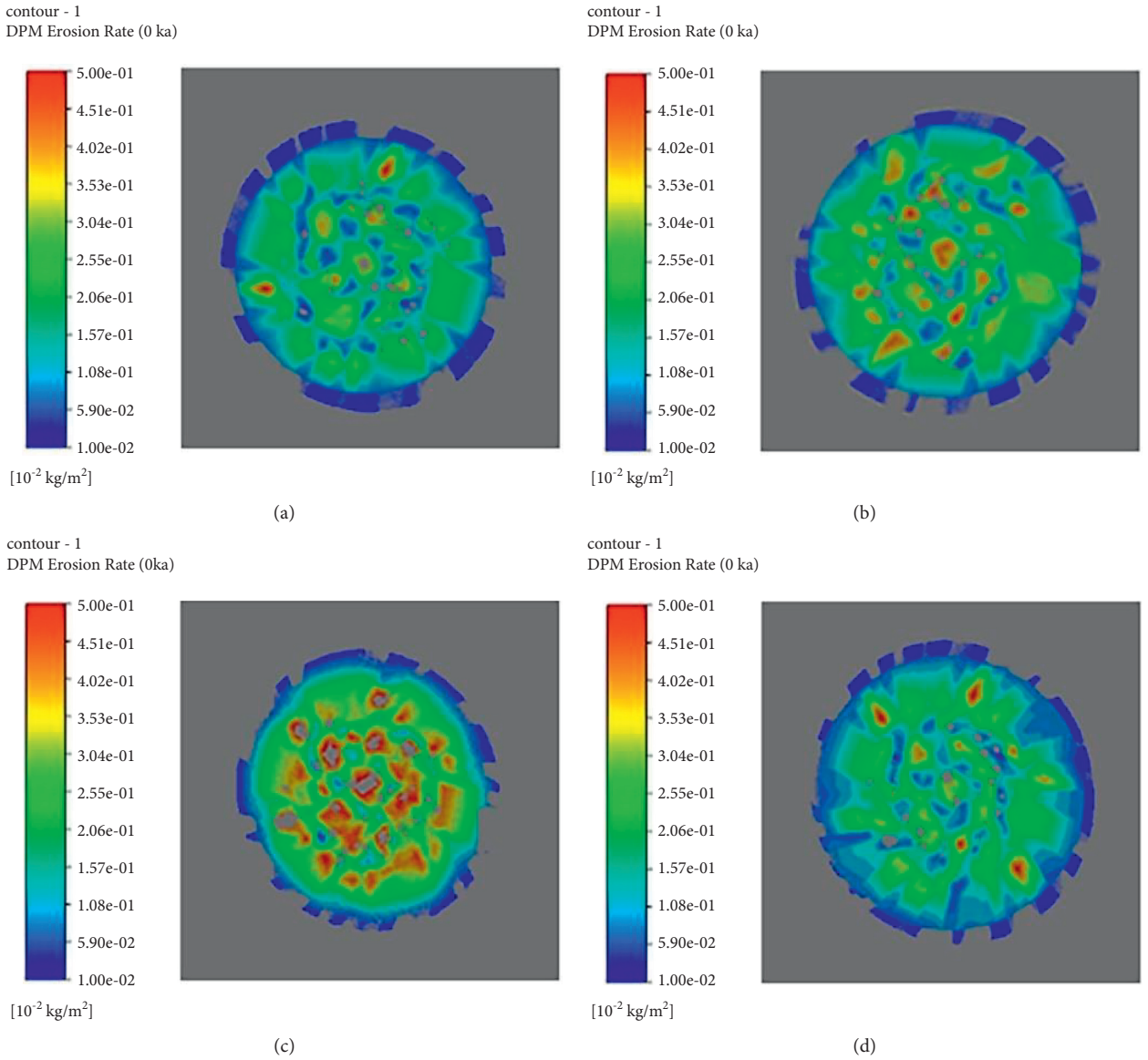

FIGURE 11: The erosion of the blade surface with different spraying distances. (a) The erosion of the blade surface with the spraying distance of 300 mm. (b) The erosion of the blade surface with the spraying distance of 400 mm. (c) The erosion of the blade surface with the spraying distance of 500 mm. (d) The erosion of the blade surface with the spraying distance of 600 mm.

Figure 15 shows the erosion results of the blade surface with the abrasive diameter of 0.2 mm, 0.3 mm, 0.4 mm, and 0.5 mm. Take the erosion with an abrasive diameter of 0.2 mm as an example. It can be seen that erosion mainly occurs in the central ring of the jet. From the shape of the erosion, it is mainly circular, which is basically consistent with the law of shear force distribution of different abrasive diameters analyzed above. At the same time, it can be seen that erosion is mainly caused by forwarding pressure and high-speed tangential force. Erosion mainly occurs in the middle and is relatively evenly distributed, which is conducive to planning and controlling the sandblasting path and realizing the uniform position of sandblasting coverage.

When the abrasive diameter is 0.3 mm, 0.4 mm, and 0.5 mm, the development law of the erosion of the blade surface is consistent with the above analysis. However, it can be seen that when the abrasive diameter is less than 0.4 mm, the erosion rate per unit area increases with the increase of the abrasive diameter, which is similar to the principle of the erosion of the blade surface. Due to the increase of abrasive diameter, abrasives have higher kinetic energy and cause greater erosion to the blade surface.

When the abrasive diameter is 0.4 mm, the erosion rate is the maximum. The abrasive obtains the maximum erosion rate under the dual action of the gas driving force and self-gravity.

However, when the abrasive diameter exceeds 0.4 mm, the erosion rate per unit area decreases with the extension of the abrasive diameter. Due to the increase of abrasive diameter, its own weight has a greater impact on the gas

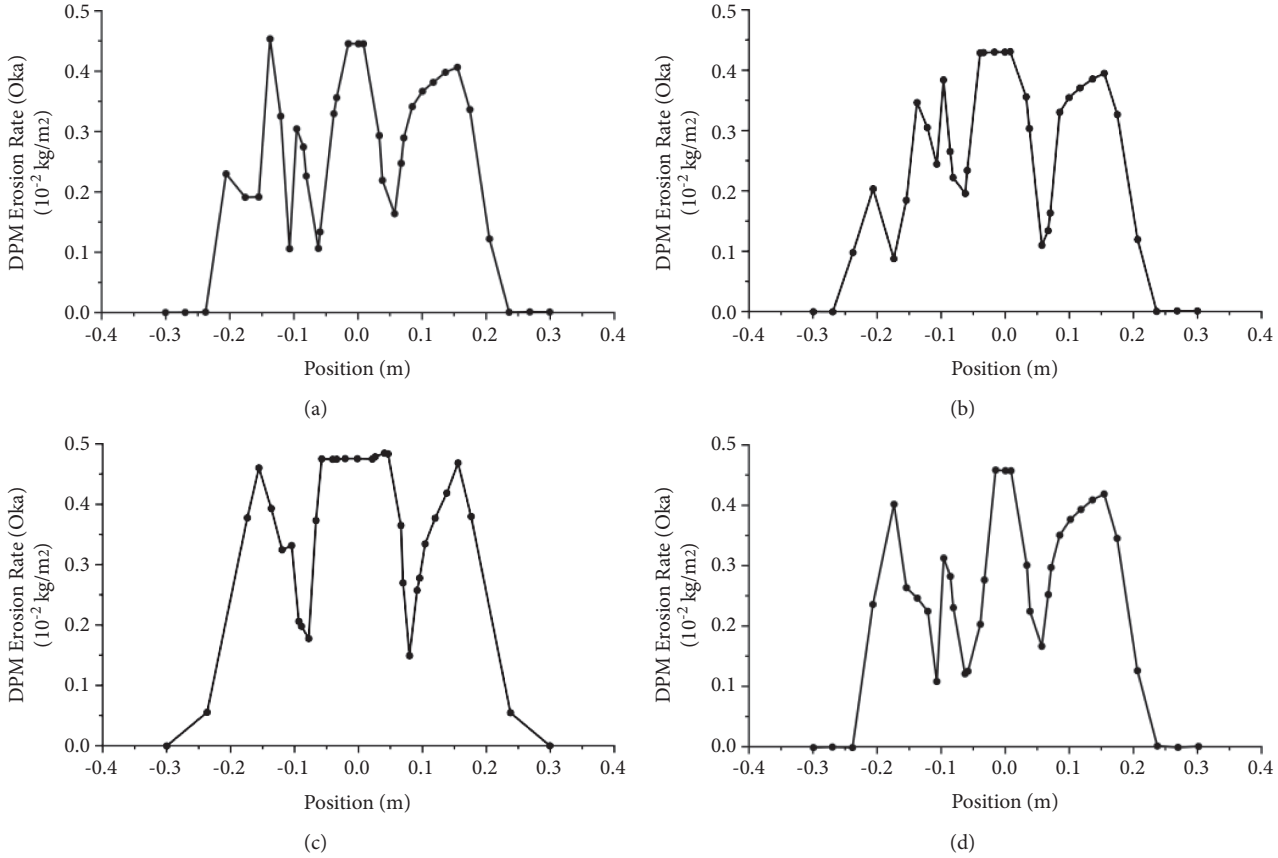

Figure 12: The erosion curve of the blade surface with different spraying distances. (a) The erosion curve of the blade surface with the spraying distance of 300 mm. (b) The erosion curve of the blade surface with the spraying distance of 400 mm. (c) The erosion curve of the blade surface with the spraying distance of 500 mm. (d) The erosion curve of the blade surface with the spraying distance of 600 mm.

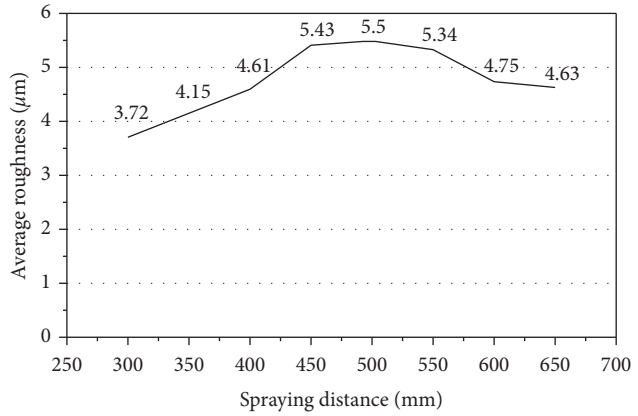

Figure 13: Average roughness curve with different spraying distances.

driving force. The decrease of driving force leads to the decrease of the velocity of abrasive and the weakening of the erosion effect of abrasive on the blade surface. At the same time, the number of abrasives reaching the blade surface per unit time decreases due to the increase of abrasive diameter. Based on the above factors, the erosion rate decreases when the abrasive diameter exceeds 0.4 mm.

Figure 16 shows the erosion curve of the blade surface when the abrasive diameter is 0.2 mm, 0.3 mm, 0.4 mm, and 0.5 mm. It can be seen that erosion also mainly occurs at the center of the jet. With the increase of abrasive diameter, the maximum erosion rate and effective erosion area are in an increasing state when the abrasive particle size is 0.2–0.4 mm. The maximum value is reached at 0.4 mm, the maximum erosion rate is 0.458×10^{-2} kg/m^2, and the effective action area is 28.5 mm^2. However, there was a decline at 0.4–0.5 mm. Due to the increase of abrasive diameter, the kinetic energy per unit abrasive increases, which can cause

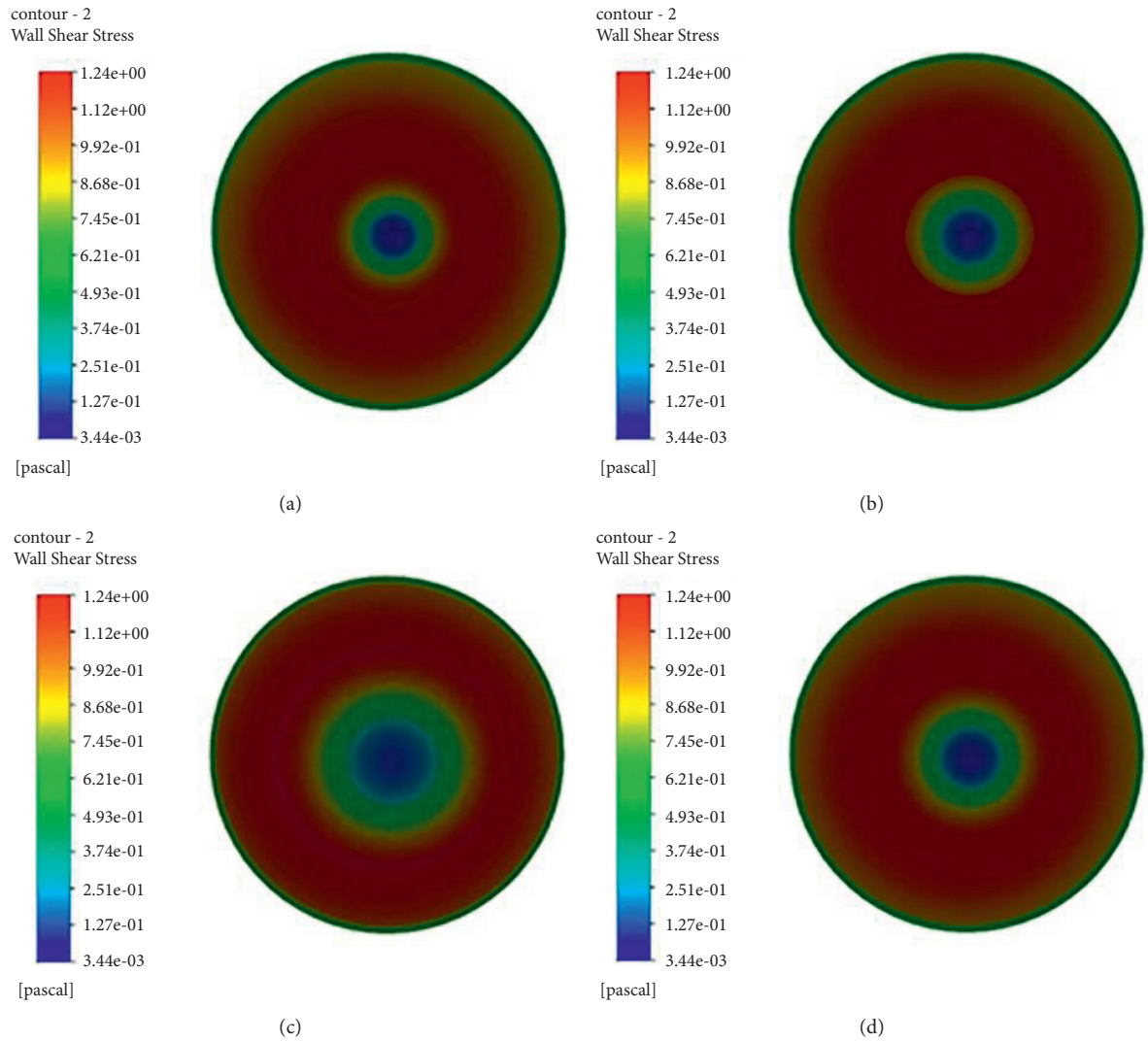

Figure 14: The shear force distribution on the blade surface with different abrasive diameters. (a) The shear force distribution on the blade surface with the abrasive diameter of 0.2 mm. (b) The shear force distribution on the blade surface with the abrasive diameter of 0.3 mm. (c) The shear force distribution on the blade surface with the abrasive diameter of 0.4 mm. (d) The shear force distribution on the blade surface with the abrasive diameter of 0.5 mm.

greater erosion to the blade surface. However, the continuous increase of abrasive diameter will increase the weight of abrasive and reduce the number of abrasives acting on the blade surface per unit time. At the same time, when the airflow pressure is constant, the compressed gas does not have enough pressure to increase its kinetic energy.

In order to compare the erosion of abrasives on the blade surface more intuitively under different abrasive diameters, the average roughness values corresponding to eight abrasive diameters are measured and counted in the simulation software. Finally, the curve is generated, see Figure 17.

When the abrasive diameter is less than 0.4 mm, the larger the abrasive diameter is, the higher the average roughness value is. The larger the abrasive diameter is, the more thrust the airflow can exert on the abrasives. Greater thrust can fully accelerate the abrasive. When the abrasives reach the jet surface, they have the highest kinetic energy.

When the abrasive diameter is more than 0.4 mm, with the larger abrasive diameter, the average roughness value decreases slowly. The average roughness value decreases slowly. With a large abrasive diameter, although the airflow has fully accelerated the abrasive, its own gravity reduces its acceleration value in the later stage. The velocity of abrasive decreases rapidly, and the kinetic energy of abrasive decreases, resulting in the reduction of erosion rate and roughness at the same time.

5. Laboratory Test

In order to verify whether the optimal parameters of the sandblasting process obtained from the simulation analysis are accurate, a laboratory test is carried out. Finally, the advantages of the optimal parameters compared with the empirical process parameters currently used are explored from the macro- and microperspectives. The measurement

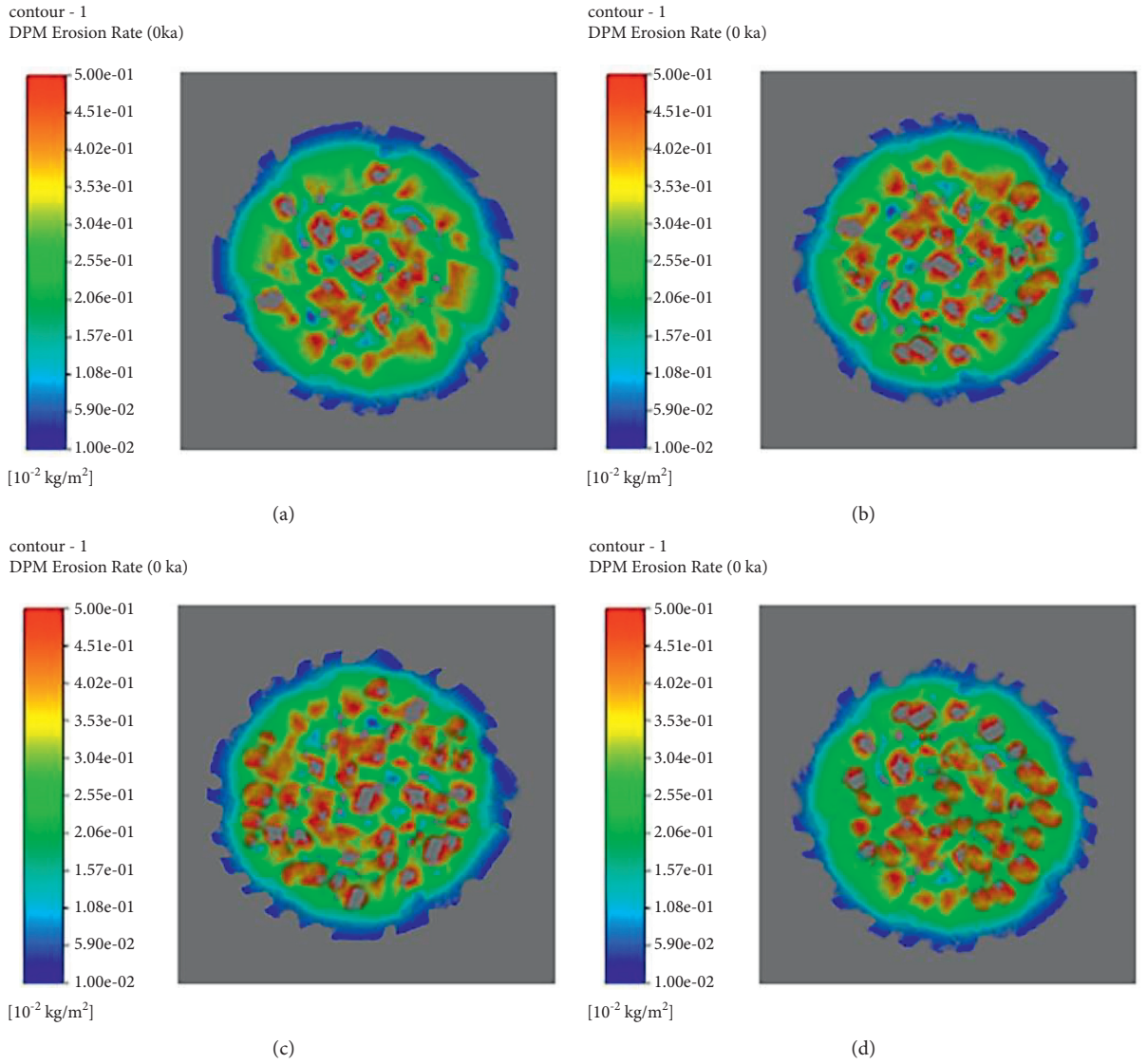

Figure 15: The erosion of the blade surface with different abrasive diameters. (a) The erosion of the blade surface with the abrasive diameter of 0.2 mm. (b) The erosion of the blade surface with the abrasive diameter of 0.3 mm. (c) The erosion of the blade surface with the abrasive diameter of 0.4 mm. (d) The erosion of the blade surface with the abrasive diameter of 0.5 mm.

division of the field test area is shown in Figure 18. The working parameters of the sandblasting machine are shown in Table 2. Observe the micromorphology of the specimens after grinding. Then, spray paint and pull-out test are carried out to compare the difference between sandblasting process and manual grinding.

During the process of sandblasting, the spray gun is 90° to the blade surface, and the sandblasting gun moves left and right within 10 cm at a speed of 0.1 m/s. The standard followed is GB/T 1720–1979 determination of film adhesion. After sandblasting, conduct a standard paint spraying operation on the test region. Then, the adhesion of the paint shall be verified and accurately recorded through the standard tensile test.

After the sandblasting operation, the surface morphology can be observed from the surface that the untreated wind turbine blades are relatively smooth and have many smooth mold marks left by post-curing. In contrast, the surface of wind turbine blades after sandblasting is obviously rough, and there are a large number of rough matte surfaces due to sandblasting. The surface drawings of wind turbine blades before and after sandblasting are shown in Figures 19(a) and 19(b), respectively.

In order to analyze the influence mechanism and impact features of the grinding process on the blade surface in detail, the treated blade surface of the specimens is observed by the electron microscope, see Figure 20. Figure 20(a) shows the specimen after manual grinding. Only resin particles passing through the felt layer of the wind turbine blade can be observed on the blade surface. It can be seen that the degree of grinding in this area is low, which will lead to a lower roughness. Figure 20(b) shows the specimen after the sandblasting process. The fiber layer of the wind turbine blade can be clearly seen on the blade surface, indicating that

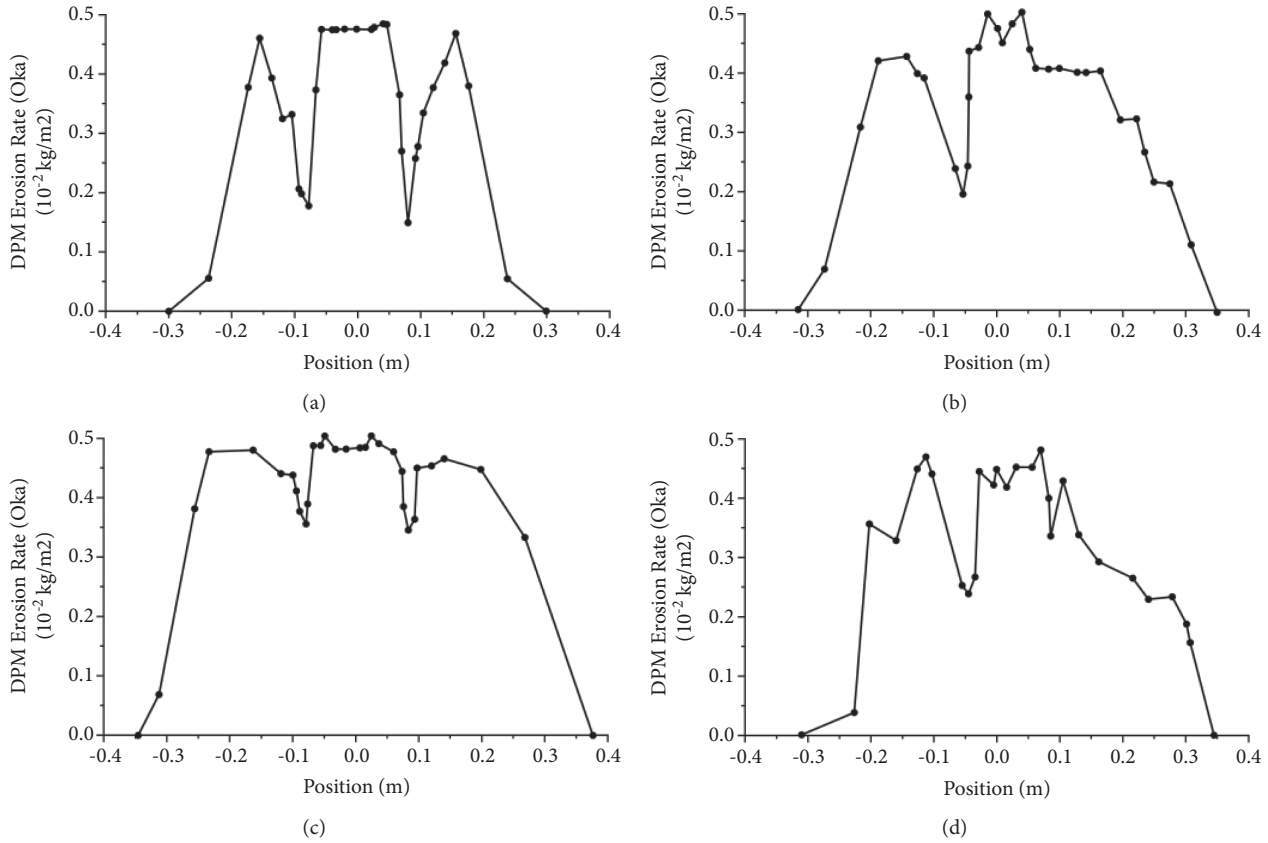

Figure 16: The erosion curve of the blade surface with different abrasive diameters. (a) The erosion curve of the blade surface with the abrasive diameter of 0.2 mm. (b) The erosion curve of the blade surface with the abrasive diameter of 0.3 mm. (c) The erosion curve of the blade surface with the abrasive diameter of 0.4 mm. (d) The erosion curve of the blade surface with the abrasive diameter of 0.5 mm.

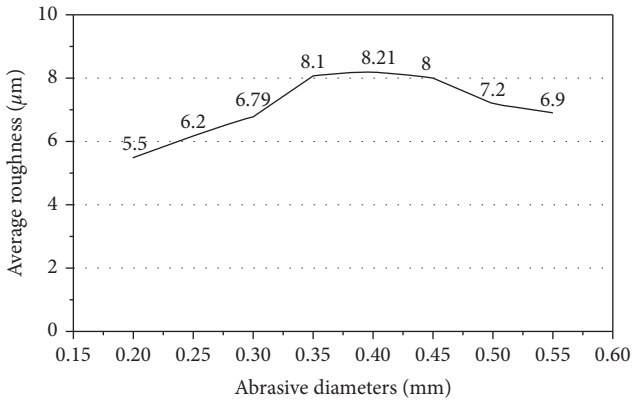

Figure 17: Average roughness curve under different abrasive diameters.

this part has a heavy sandblasting treatment, which will lead to a higher roughness.

Conduct tensile tests on the specimens under the same force level until the paint falls off. Then, collected test date and paint failure details are shown in Figure 21.

The tensile strength of the manual ground wind turbine blade surface is 7.68 MPa. The tensile strength of the wind turbine blade surface after sandblasting process is 8.36 MPa.

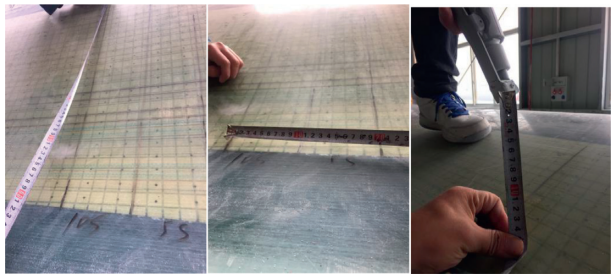

Figure 18: Division of test region.

Table 2: Main working parameters of sandblasting machine.

Name	Value
Air volume	50 m^3/min
Sand absorption capacity	3–8 T/H
Maximum vacuum	−0.0667 Mpa
Sand loading	4000 kg
Working pressure	0.4–1.2 Mpa
Compressed air consumption	>6 m^3/min
Work efficiency	≥15 m^2/h
Spraying distance	<2.4 m
Abrasive diameter	<0.8 mm

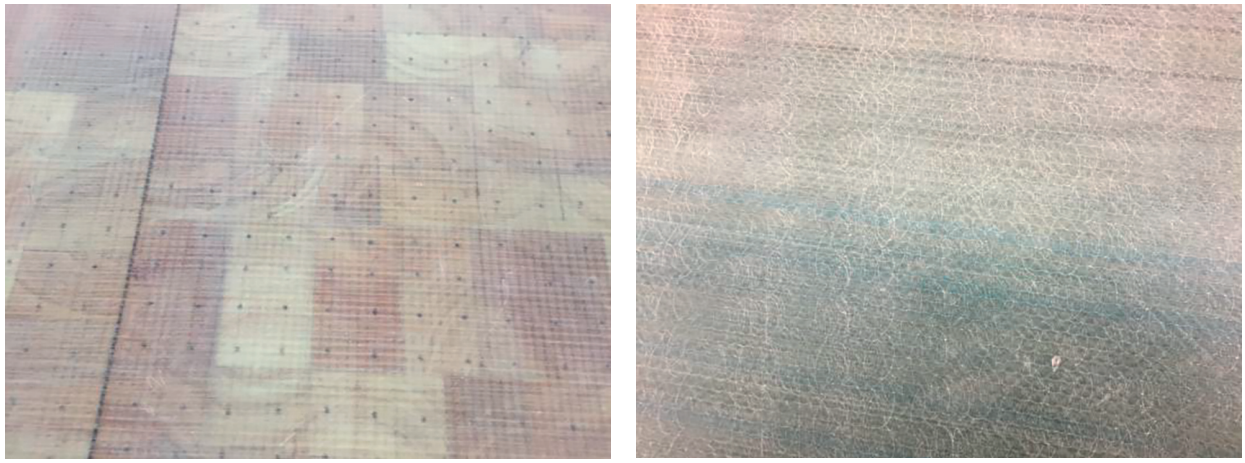

(a) (b)

Figure 19: (a). Blade surface before sandblasting. (b). Blade surface after sandblasting.

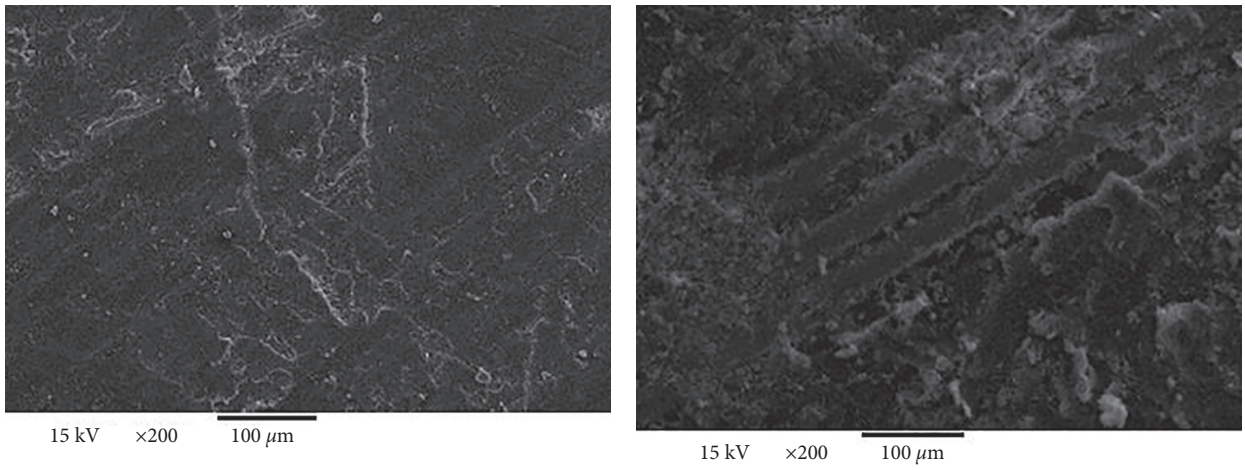

(a) (b)

Figure 20: Electron microscope of the specimens after grinding. (a) Electron microscope of the specimen after the manual grinding process. (b) Electron microscope of the specimen after sandblasting process.

The sandblasting process can effectively improve the adhesion of the coating. Stronger paint coating adhesion can improve the ability of wind turbines to deal with severe environmental erosion such as wind sand and seawater.

6. Discussion

The surface properties of the material ground through the sandblasting process have been improved. And the sandblasting process will not affect the mechanical properties of the sample itself. This conclusion is the same as that in [17, 18]. More conclusions on blade grinding working parameters are as follows.

6.1. Optimum Blasting Pressure. In the range of 0.5–0.8 MPa, the speed of airflow and the speed of abrasive reaching the blade surface will increase with the increase of pressure. The increase of abrasive velocity will change the action region of forwarding pressure and tangential force of abrasive on the blade surface. At the same time, the simulation shows that the erosion effect of abrasive on the blade surface is mainly caused by forwarding pressure and high-speed tangential force. However, it can be seen from the erosion of the blade surface that when it is lower than 0.7 MPa, the erosion rate and average roughness value increase with the increase of abrasive velocity. When the blasting pressure exceeds 0.7 MPa, the erosion rate and average roughness value begin to decline with the increase of pressure.

In a certain range, the abrasive has higher kinetic energy and the erosion effect is strengthened with the increase of blasting pressure. When a certain pressure is exceeded, the flow of compressed gas will affect the flow beam shape of abrasive, which will lead to the convergence of flow beams and the decline of erosion rate and average roughness. Through the above analysis, it can be determined that 0.7 MPa is the best blasting pressure in the pressure range of 0.5–0.8 MPa.

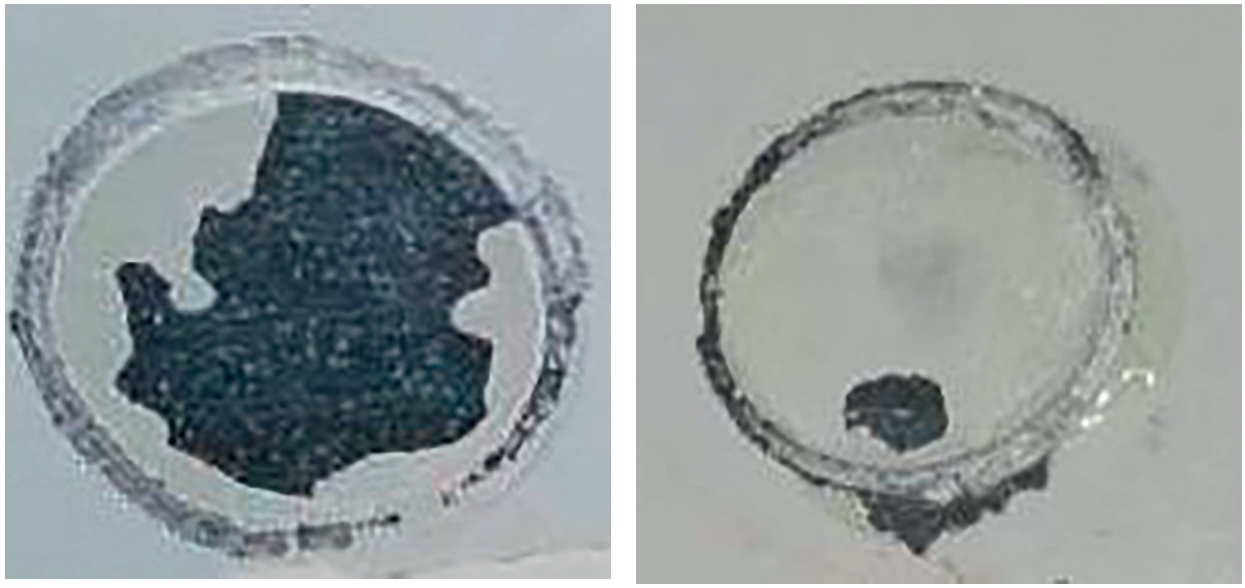

7.68 MPa

(a)

8.36 MPa

(b)

Figure 21: The paint of the specimens after tensile tests. (a) The paint of the specimen after the manual grinding process. (b) The paint of the specimen after sandblasting process.

6.2. Optimum Abrasive Diameter. When the abrasive diameter is in the range of 0.2–0.4 mm, the abrasive velocity continues to increase with the increase of abrasive diameter under the same pressure and spraying distance, and the erosion rate and average roughness increase at the same time. The increase of abrasive diameter leads to the increase of windward area, and the gas exerts a higher driving force on the abrasive, making it have higher kinetic energy. In the range of 0.4–0.5 mm, the abrasive erosion speed, erosion rate, and average roughness decrease with the increase of abrasive diameter. Although the abrasive obtains a higher driving force due to the increase of its diameter, the adding of abrasive diameter increases its weight and reduces the number of abrasives emitted per unit time. Therefore, compressed air does not have enough pressure to increase the kinetic energy of abrasive. Therefore, 0.4 mm is the best abrasive particle size in the range of abrasive diameter of 0.2–0.5 mm.

6.3. Optimum Spraying Distance. In the range of spraying distance of 300–600 mm, the gas velocity first increases and then decreases rapidly with the increase of spraying distance. From the shear stress distribution cloud diagram, the region of the effective erosion rate increases with the increase of spraying distance, and the maximum value appears at 500 mm. However, the area of the effective erosion rate decreases in the process of 500–600 mm. Due to expansion, the compressed gas will continue to accelerate within a certain distance from the nozzle. However, the velocity of gas will decrease significantly after accelerating to a certain distance with the disappearance of the potential nucleus. The change of compressed air velocity also leads to the change of abrasive velocity. Finally, due to the decrease of abrasive kinetic energy, the erosion effect of abrasive on the blade surface decreases. Therefore, 500 mm is the best spraying distance in the range of 30–600 mm.

7. Conclusion

In this study, blasting pressure, abrasive diameter, and sandblasting distance are simulated with erosion rate and average roughness as the main evaluation indexes. The sandblasting erosion mechanism of the wind turbine blade surface is analyzed and some conclusions can be drawn.

In the range of sandblasting pressure of 0.5–0.8 MPa, spraying distance of 300–600 mm, and abrasive diameter of 0.2–0.5 mm, the best combination of sandblasting parameters is sandblasting pressure of 0.7 MPa, the abrasive diameter of 0.4 mm, and spraying distance of 500 mm.

The surface roughness of blades affects the reliability of paint. Under appropriate working parameters, the reliability of composite paint polished by sandblasting process is better than that polished by manual.

Data Availability

The material properties and the data of the tensile test used to support the findings of this study were supplied by Lianyungang ZhongfuLianzhong Composites Group CO., LTD, and they are included within the article.

Conflicts of Interest

The authors declare that they have no conflicts of interest.

Acknowledgments

This research was funded by National Key R&D Program of China (Grant no. 2018YFB1501203) and Natural Science Foundation of Shandong (Grant no. ZR2019MEE076). The work has partly received funding from National Key R&D Program of Shandong (Grant no. 2019GGX104001).

References

[1] X. U. Yu, C. C. Liao, S. L. Zhang, S. U. Xiangying, and X. L. Zhao, "Developing trend of design and manufacture technology for large-scale wind turbine blade," *SCIENTIA SINICA Physica, Mechanica & Astronomica*, vol. 46, no. 12, p. 124702, 2016.

[2] M. Damiano, A. Russo, A. Sellitto, E. Vecchio, T. Stellato, and A. Riccio, "Design of a composite wind turbine blade manufactured with the ONE SHOT BLADE technology," *Materials Today Proceedings*, vol. 34, pp. 103–105, 2021.

[3] F. Mølholt Jensen and K. Branner, "Introduction to wind turbine blade design," In: P. Brøndsted and R. Nijss, *Advances in Wind Turbine Blade Design and Materials*, Woodhesd Publishing, Sawston, UK, pp. 3–28, 2013.

[4] K. Dathu and R. Hariharan, "Design of wind turbine blade material for higher efficiency," *Materials Today Proceedings*, vol. 33, pp. 565–569, 2020.

[5] C. Chen, J. Wang, H. Huang, and S. Wang, "Study on test method for anti-icing performance of anti-icing paint for wind turbine blade," *Paint & Coatings Industry*, vol. 46, no. 06, pp. 56–60, 2016.

[6] K. J. Disotell, P. Nikoueeyan, J. W. Naughton, and J. W. Gregory, "Application of fast pressure-sensitive paint to an oscillating wind turbine airfoil," *2015 North American Wind Energy Academy*, Blacksburg, Commonwealth of Virginia, Blacksburg, VA, USA, 2015.

[7] K. J. Disotell and J. Gregory, "Time-resolved measurements of cellular separation on a stalling airfoil," in *Proceedings of the 53rd AIAA Aerospace Sciences Meeting*, Reston, VA, January 2015.

[8] Q. Miao, W. Ding, W. Kuang, and C. Yang, "Grinding force and surface quality in creep feed profile grinding of turbine blade root of nickel-based superalloy with microcrystalline alumina abrasive wheels - sciencedirect," *Chinese Journal of Aeronautics*, vol. 34, no. 2, pp. 576–585, 2019.

[9] X. Li, J. Nan, X. Zhou, H. Liang, and C. Yue, "Quality comparison of grinding surface and milling surface for 17-4ph turbine blade root," *Tool Engineering*, vol. 52, no. 1, pp. 30–33, 2018.

[10] D. S. Cousins, Y. Suzuki, R. E. Murray, J. R. Samaniuk, and A. P. Stebner, "Recycling glass fiber thermoplastic composites from wind turbine blades," *Journal of Cleaner Production*, vol. 209, no. 1, pp. 1252–1263, 2019.

[11] V. A. Poletaev and E. V. Tsvetkov, "Improvements in turbine-blade manufacture," *Russian Engineering Research*, vol. 38, no. 12, pp. 1053–1055, 2018.

[12] K. Maruyama, Y. Eto, and Y. Kishimoto, *Method for Grinding Tip of Rotor Blade, and Jig for Grinding Tip of Blisk*, US20180339390, 2018.

[13] L. U. Gaofeng, W. U. Qiang, X. U. Qingping, and W. U. Guoxing, "Development of electrolytic and cutting combined grinding equipment for hair-cutting blade edge," *Electromachining & Mould*, vol. 2, pp. 39–41, 2018.

[14] A. S. Verma, N. P. Vedvik, and Z. Gao, "A comprehensive numerical investigation of the impact behaviour of an offshore wind turbine blade due to impact loads during installation," *Ocean Engineering*, vol. 172, pp. 127–145, 2019.

[15] A. S. Verma, Z. Jiang, N. P. Vedvik, Z. Gao, and Z. Ren, "Impact assessment of a wind turbine blade root during an offshore mating process," *Engineering Structures*, vol. 180, no. 1, pp. 205–222, 2018.

[16] D. Kirk and M. Y. Abyaneh, "Theoretical basis of shot peening coverage control," *The Shot Peener*, vol. 2, no. 9, pp. 28–30, 1995.

[17] B. Suyitno Arifvianto, T. D. Widodo, M. Mahardika, and P. Dewo, "Effect of cold working and sandblasting on the microhardness, tensile strength and corrosion resistance of aisi 316l stainless steel. International Journal of Minerals," *Metallurgy and Materials*, vol. 19, no. 12, p. 7, 2012.

[18] A. Singh, S. Ghosh, and S. Aravindan, "Influence of dry micro abrasive blasting on the physical and mechanical characteristics of hybrid PVD-AlTiN coated tools," *Journal of Manufacturing Processes*, vol. 37, pp. 446–456, 2019.

[19] D. Draganovská, G. Ižaríková, A. Guzanová, and J. Brezinová, "General Regression model for Predicting surface Topography after abrasive blasting," *Metals*, vol. 8, no. 11, p. 938, 2018.

[20] H. Singh, L. Rai, and S. R. Kale, "A numerical study of the effect of roughness on the turbine blade cascade performance. Progress in Computational Fluid Dynamics," *International Journal*, vol. 8, no. 7-8, p. 439, 2008.

[21] K. Shiyuan, Li Xinmei, School of Mechanical Engineering, and Xinjiang University, "Numerical simulation study on erosion wear of wind turbine blade materials," *Rural Energy*, vol. 5, pp. 656–661, 2015.

[22] S. Zhang, K. Dam-Johansen, S. Nørkjær, P. L. Bernad, and S. Kiil, "Erosion of wind turbine blade coatings - design and analysis of jet-based laboratory equipment for performance evaluation," *Progress in Organic Coatings*, vol. 78, pp. 103–115, 2015.

[23] B. Amirzadeh, A. Louhghalam, M. Raessi, and M. Tootkaboni, "A computational framework for the analysis of rain-induced erosion in wind turbine blades, part II: drop impact-induced stresses and blade coating fatigue life," *Journal of Wind Engineering and Industrial Aerodynamics*, vol. 163, pp. 44–54, 2017.

[24] Q. Miao, W. Ding, W. Kuang, and C. Yang, "Grinding force and surface quality in creep feed profile grinding of turbine blade root of nickel-based superalloy with microcrystalline alumina abrasive wheels," *Chinese Journal of Aeronautics*, vol. 34, no. 2, pp. 576–585, 2021.

[25] Z. Li, L. Zou, J. Yin, and Y. Huang, "Investigation of parametric control method and model in abrasive belt grinding of nickel-based superalloy blade," *International Journal of Advanced Manufacturing Technology*, vol. 108, no. 9-10, pp. 3301–3311, 2020.